# Electroconvection in one-dimensional liquid crystal cells

Jong-Hoon Huh
*Department of Mechanical Information Science and Technology, Faculty of Computer Science and Systems Engineering, Kyushu Institute of Technology, Fukuoka 820-8502, Japan*

(Received 16 January 2018; published 30 April 2018)

We investigate the alternating current (ac) -driven electroconvection (EC) in one-dimensional cells (1DCs) under the in-plane switching mode. In 1DCs, defect-free EC can be realized. In the presence and absence of external multiplicative noise, the features of traveling waves (TWs), such as their Hopf frequency $f_H$ and velocity, are examined in comparison with those of conventional two-dimensional cells (2DCs) accompanying defects of EC rolls. In particular, we show that the defects significantly contribute to the features of the TWs. Additionally, owing to the defect-free EC in the 1DCs, the effects of the ac and noise fields on the TW are clarified. The ac field linearly increases $f_H$, independent of the ac frequency $f$. The noise increases $f_H$ monotonically, but $f_H$ does not vary below a characteristic noise intensity $V_N^*$. In addition, soliton-like waves and unfamiliar oscillation of EC vortices in 1DCs are observed, in contrast to the localized EC (called worms) and the oscillation of EC rolls in 2DCs.

DOI: 10.1103/PhysRevE.97.042707

## I. INTRODUCTION

Alternating current (ac) -driven electroconvection (EC) has been extensively investigated—along with thermal convection, which is more widely known—to understand the pattern-formation physics of nonequilibrium systems [1–3]. In general, EC can be induced in liquid crystals by applying an electric field across their thin layer (typically, $d = 10-100\,\mu$m). Because of the simplicity of the theory and experiments for EC, nematic liquid crystals (NLCs) characterized by the uniaxial orientation of the calamitic molecules are typically used [4]. The basic mechanism of EC was satisfactorily explained in studies by Carr [5] and Helfrich [6] and was more generally treated by Bodenschatz *et al.* [7]. In principle, the director fluctuations of the NLC resulting from thermal fluctuations can be reinforced by a material flow owing to the Coulomb force acting on space charges, which are focused by the electric anisotropy of the NLC. When the Coulomb force overcomes the viscoelastic and dielectric restoring forces at a critical voltage $V_c$, electrohydrodynamic instability arises in the NLC layer, and EC occurs. However, there are various EC structures and dynamics beyond the basic mechanism determining a stationary, periodical roll pattern [i.e., the Williams domain (WD)] [8]. Generally, one can observe stationary, oscillatory, or spatiotemporal chaotic features in the EC, depending on (i) the initial boundary conditions for the director; (ii) the main control parameters, i.e., the voltage $V$ and frequency $f$; (iii) the main material parameters, such as the conductivity and dielectric constants, as well as their anisotropy; and (iv) other effects of the NLC, such as flexoelectricity [4,9]. Therefore, owing to the details of the experimental conditions, including uncontrollable factors, unexpected EC patterns have frequently been observed with the typical WD [9].

In this paper, an oscillatory EC observed as traveling waves (TWs) is presented, which cannot be explained by the basic Carr-Helfrich mechanism [5,6]. Fortunately, however, the TW was successfully explained by the weak-electrolyte model (WEM) suggested by Treiber and Kramer [10]. In the WEM, under the new feasible assumption of the dissociation and recombination of neutral molecules (and also impurities or dopants) in the EC system, the constant Ohmic conductivity ($\sigma$) was replaced by a variable $\sigma(\boldsymbol{r},t)$. Indeed, the local deviation of the conductivity $[\sigma(\boldsymbol{r},t) - \sigma]$ from its equilibrium value ($\sigma$) couples to the director field and has a stabilization effect against the primary Carr-Helfrich destabilization effect. The interplay between such reciprocal effects can generate oscillatory instability (i.e., TW) [10]. Additionally, the WEM has been reconsidered in a more general activator-inhibitor model showing Hopf bifurcation: the local deviation of the conductivity and the deformation of the director field play roles as an activator and an inhibitor, respectively [11].

Recently, the effects of noise on EC have been intensively examined, with the aim of controlling the threshold of EC [12,13]. Furthermore, additional ac or direct-current fields have been used for such control [9]. We recently reported a TW in the presence of noise superposed on the ac field [11]; in particular, we discovered that noise can generate a TW from a stationary wave (SW), foster the activeness of the TW (i.e., the Hopf frequency of the TW), and even induce localized waves (called "worms") [14]. Moreover, the roles of the ac and noise fields have been discussed with the demonstration of pattern evolutions under the variation of both fields [11]. In our previous experiments, we used conventional two-dimensional cells (2DCs) having large aspect ratios (typically $10^3 - 10^4$) with respect to the thickness of the NLC layer. In 2DCs, defects of EC rolls appear because of the various instabilities beyond $V_c$; in particular, the climb, glide, and oscillation of defects change the structures and dynamics of EC [15,16]. In the situation where defects appear in the TW, unexpected competition between traveling rolls by the WEM and modulating rolls due to the motion of defects determines the features of the TW [11]. Consequently, the effect of the WEM cannot be accurately

 

evaluated unless the contribution of defects is separated from the TW. For this reason, we prepared a unique EC cell by employing the "in-plane switching mode," which is well-known in application research on liquid-crystal devices [4,17,18]. Thus, one-dimensional cells (1DCs) providing defect-free EC were realized [19].

To elucidate the present experimental findings on TWs in 1DCs, we summarize the previous results observed in 2DCs where the same NLC was used [11]: (i) the Hopf frequency $f_H$ for TWs was relatively low ($f_H < 1$ Hz) compared with that for a 1DC ($f_H < 20$ Hz; see below); (ii) in most cases, TW-accompanied defects and the motion of defects inhibited the activeness of TWs, reducing $f_H$; (iii) a beating TW showing amplitude modulations often appeared; (iv) TW sustained at high noise intensities deviated from the prediction of the WEM; and (v) a localized TW called worms was induced by high noise intensities.

In this study, we focus on the TW in a 1DC under noise superposed on the ac field, as well as under a pure ac field. The Hopf frequency of the TW is intensively examined via dynamic image analysis and compared with previous results observed for 2DCs [11]. One can observe the effects of defects in 2DCs via comparison with the results obtained for a 1DC giving defect-free EC; thus, the effects of the ac and noise fields on the TW can be clarified. In addition, various patterns and dynamics of EC in a 1DC are presented, some of which are quite noticeable for the current pattern-formation physics of nonequilibrium systems.

## II. EXPERIMENT

A well-known typical NLC [*p*-methoxybenzylidene-*p*′-*n*-butylaniline (MBBA)] was used for EC. The following were measured for the NLC: a conductivity of $\sigma_\perp = 2.01 \times 10^{-8}\,\Omega^{-1}\,\mathrm{m}^{-1}$, a dielectric constant of $\varepsilon_\perp = 5.14$ (at $T = 25\,^\circ$C), anisotropy of $\sigma_a = \sigma_\parallel - \sigma_\perp = 6.21 \times 10^{-8}\,\Omega^{-1}\,\mathrm{m}^{-1}$, and $\varepsilon_a = \varepsilon_\parallel - \varepsilon_\perp = -0.35$. Here $\parallel$ and $\perp$ denote the orientations parallel and perpendicular to the initial director $\boldsymbol{n}_0$, respectively. Figure 1 shows the present 1DC prepared by employing the in-plane switching mode [Fig. 1(d)] and a typical EC pattern in the 1DC [Fig. 1(b)]. Note that $E(t) = (\sqrt{2}V/d)\sin 2\pi f t$ is applied to the NLC in the 1DC [Fig. 1(d)], in contrast to $\boldsymbol{E}(t) = E(t)\hat{\boldsymbol{z}}$ for the conventional 2DC [4–10]; commercial "comb-type" evaluation cells with transparent electrodes (indium tin oxide) were used (E.H.C. Co.). In principle, the EC in a 1DC having vortices [Fig. 1(c)] is consistent with that in the side-view cells called Hele-Shaw cells [20]; thus, it is very similar to the side-view WD (Fig. 2 in Ref. [20]). Furthermore, to examine the effects of noise on the EC, Gaussian-type electric noise $\xi(t)$ was superposed on $E(t)$ ($\boldsymbol{\xi} \parallel \boldsymbol{E}$). The (deterministic) ac voltage $V = d\sqrt{\langle E^2(t)\rangle}$ with a frequency of $f$ ($= 10 - 500$ Hz) and the (stochastic) noise intensity $V_N = d\sqrt{\langle \xi^2(t)\rangle}$ with a cutoff frequency $f_c = 200$ kHz were used as the main control parameters. The standard shadowgraph method was used for optical observations and measurements [4,11]; the EC patterns and their dynamics were observed by using a computer-controlled image software (Scion Image) and an image-capture board (Scion Corp., PCI-VE5) together with a charge-coupled device camera (Sony, XC-75) mounted on a polarizing microscope

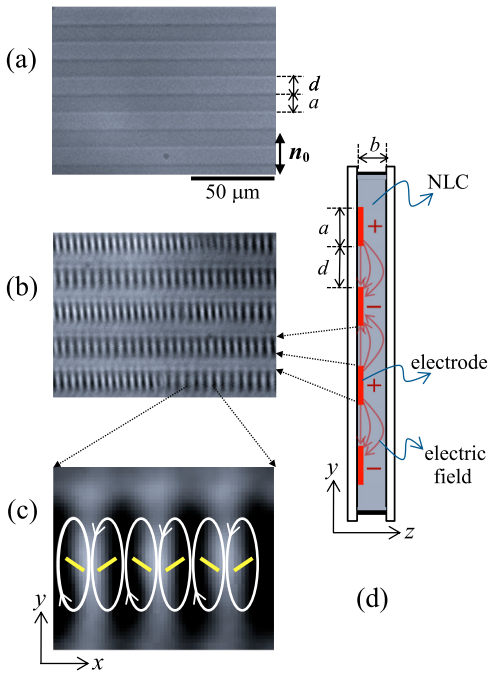


FIG. 1. EC in a 1DC prepared by employing the in-plane switching mode. (a) Picture of the cell in the $xy$ plane (with an electrode width of $a = 10\,\mu$m, a gap of $d = 10\,\mu$m between electrodes, and an electrode thickness of $\Delta z \approx 0.16\,\mu$m). The active dimensions for EC were $L_x \times L_y = 1 \times 1$ cm. (b) Typical EC pattern (at $V = 45.2$ V and $f = 200$ Hz), (c) Scheme of EC in the 1DC, (d) 1DC depicted in the $yz$ plane. The slab of an NLC is $b = 50\,\mu$m. The thick rods and ellipsoids in (c) indicate the director $\boldsymbol{n}(x,y)$ of the NLC and the EC vortices, respectively; $\boldsymbol{n}_0$ denotes the initial director of the NLC ($\boldsymbol{n}_0 \parallel \boldsymbol{E} \parallel \hat{\boldsymbol{y}}$ at the surface). Ac-driven EC is induced between electrodes by applying a voltage above the critical voltage $V_c$.

(Meijitech, ML9300) [11]. All measurements (except for Figs. 10 and 11) were performed at a fixed temperature of $T = 25\,^\circ$C using an electrothermal control system (TH-99, Japan Hightech).

## III. RESULTS AND DISCUSSION

### A. Phase diagram in frequency-voltage plane

The optical patterns that we observed in the 1DC can be distinguished from those found in 2DCs [3–13]. Figure 2(g) shows threshold voltages for the patterns in the $f$-$V$ plane, although these lines are roughly estimated, except the $V_c$ for the onset of EC, which is indicated by solid circles. For low frequencies below a certain characteristic frequency $f_d$ (approximately 50 Hz), a (transient) disclination pattern [Fig. 2(e)] occurs owing to the dielectric deformation of the director field ($\boldsymbol{n}$) through twofold degeneracy breaking between $\boldsymbol{E}$ and $\boldsymbol{n}$; that is, two angles $+\phi$ or $-\phi$ between $\boldsymbol{E}$ and $\boldsymbol{n}$ are achievable in the free energy of the director deformation, $-(1/2)\varepsilon_0\varepsilon_a\cos^2\phi E^2$. This situation is similar to the Fréedericksz transition in a 2DC with homeotropic alignment ($\boldsymbol{E} \parallel \boldsymbol{n}_0$) [4,9,21]; thus, Fig. 2(e) in the 1DC corresponds to the well-known Schlieren textures in 2DCs [21]. After the appearance of the disclination pattern, EC [Fig. 2(d)] appears at a threshold voltage $V_c$. The weakly developed EC [Fig. 2(d)] in the disclination structure of the

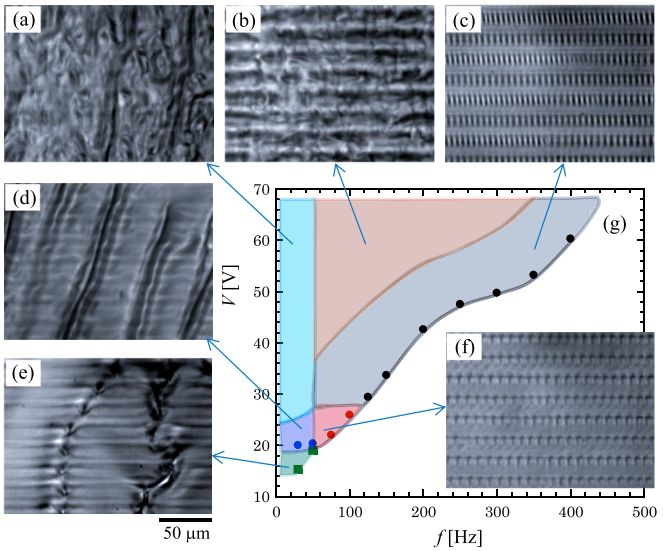


FIG. 2. Phase diagram and various patterns in the 1DC. (a) Well-known DSM. (b) Typical DSM in the 1DC [distinguished from (a)], (c) TWs, (d) EC on disclination patterns. (e) Disclination patterns before EC, (f) SWs. (g) Phase diagram in the ac-frequency and voltage plane. The horizontal pattern in (e) may be caused by the small declination of the director resulting from the electric field [including the effect of small electric-field gradients shown in Fig. 1(d)].

NLC is observed for narrow voltage ranges ($>V_c$). Beyond these ranges, turbulence [Fig. 2(a)] arises, which corresponds to the dynamic scattering mode (DSM) found in 2DCs [9,22].

On the other hand, for an intermediate frequency range ($f_d < f < f_{TW} \approx 120$ Hz), EC showing SWs [Fig. 2(f)] occurs at $V_c$ and then evolves into traveling EC [i.e., TWs, as shown in Fig. 2(c)] with increasing $V$. Eventually, at a high $V$, turbulent EC [Fig. 2(b)] appears, but it can be distinguished from that [Fig. 2(a)] observed at low frequencies ($<f_d$); i.e., it strongly reflects one-dimensional EC. Furthermore, for high frequencies above a certain characteristic frequency $f_{TW}$ (approximately 120 Hz), TW arises at $V_c$ as a primary instability and then develops into the turbulent EC [Fig. 2(b)] with increasing $V$. Such a frequency $f_{TW}$ dividing SWs and TWs was also observed in a 2DC in our recent study [11]; it played a critical role in the features of the TWs and pattern-evolution scenarios including TWs [11]. Although many interesting and unknown characteristics of EC have been observed in 1DCs, TWs [Fig. 2(c)] and SWs [Fig. 2(f)] are mainly considered in this paper to achieve our aims.

### B. Features of TWs

Figure 3 shows the features of the TW found in the 1DC. A space-time map (STM) was constructed by successively placing a one-pixel line ($X$) arbitrarily selected in active EC lanes [e.g., Fig. 1(b)] with an identical time interval ($\Delta t = 0.033$ s in this study). The angle $\theta$ of the slope for the gray lines in the STM [Fig. 3(a)] implies the velocity $v$ of the TW ($\theta \neq 0$); if $\theta = 0$, the EC is an SW with $v = 0$ (and $f_H = 0$). Furthermore, a right-TW (RTW) and a left-TW (LTW) arise with $-\pi/2 < \theta < 0$ and $0 < \theta < \pi/2$, respectively. Therefore, a larger $|\theta|$ yields faster TW

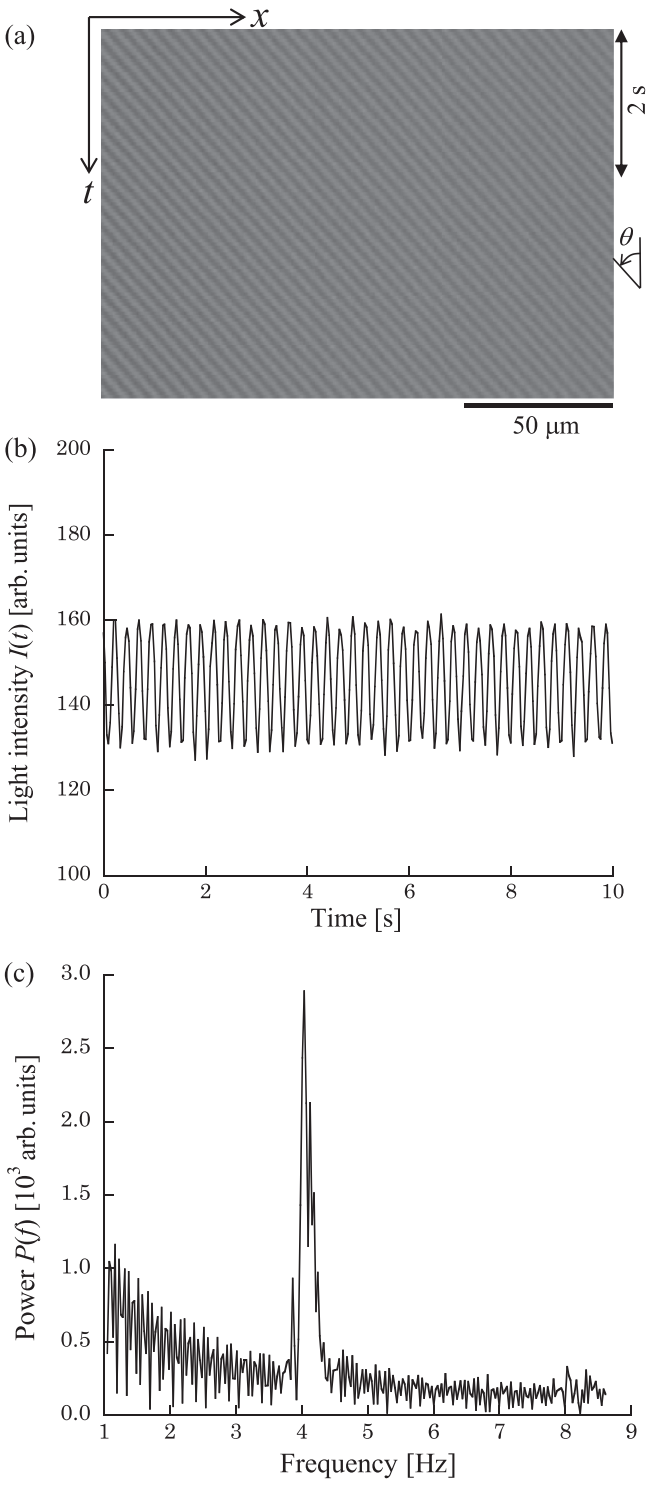


FIG. 3. STM and Hopf frequency for TW. (a) Typical STM obtained by successive placement of the one-line image $X$ with an identical time interval $\Delta t = 0.033$ s. A right-TW (RTW with $\theta < 0$) is distinguishable from the SW ($\theta = 0$). (b) Transmitted light intensity $I(t)$ for a TW obtained at an arbitrarily selected point $x_0$ in (a), (c) Calculated power spectra from (b) for an example. The peak in (c) indicates the Hopf frequency $f_H$ (approximately 4 Hz) of the TW.

movement. The regularity in Fig. 3(a) indicates a typical RTW (without defects) that maintains its constant (phase) velocity; accordingly, the transmitted light intensity $I(t)$ measured at an

arbitrary position $x_0$ in the STM exhibits a periodicity (i.e., $1/f_H$) in Fig. 3(b). The peak of $I(t)$ is directly related to the amplitude $A_R$, which is nearly constant. Thus, as shown in Fig. 3(c), the Hopf frequency $f_H$ of the TW can be determined: e.g., $f_H \approx 4$ Hz. The difference in the TW features between the 1DC and 2DC has been clarified; in particular, the regularity of the STM for the TW without defects and the extent of $f_H$ are remarkably distinguished from those found in the 2DC (e.g., Fig. 2 in Ref. [11]). The difference of the extent of $f_H$ between the 1DC and 2DC may originate from the distance $d$ between the two electrodes for EC. Considering the prediction of the WEM ($f_H \propto \sigma^{-1/2} d^{-3}$), an $f_H(1DC)/f_H(2DC)$ value of $10-10^2$ is experimentally estimated, which is roughly consistent with $[d(1DC)/d(2DC)]^{-3} = (10\,\mu m/50\,\mu m)^{-3} \approx 10^2$. This means that the WEM works well in the present 1DC.

### C. Voltage-dependent TWs

We examined the dependence of the TW on the ac voltage $V$. For $f = 100$ Hz ($< f_{TW} \approx 120$ Hz), an STM was constructed with a steplike increase of $V$, as shown in Fig. 4. Obviously, an SW ($\theta = 0$) was induced as a primary instability at $V_c = 24.1$ V, which evolved into an LTW ($\theta > 0$) at $V = 28.2$ V owing to a secondary instability [see also Fig. 2(g)]. A higher applied $V$ leads to faster movement of the LTW ($\theta \gg 0$) after the SW-TW transition; that is, $f_H$ increases with $V$. On the other hand, for $f = 200$ Hz ($> f_{TW}$), another STM was obtained via the same method, as shown in Fig. 5. An RTW ($\theta < 0$) suddenly arises as a primary instability at $V_c = 38.4$ V; no SW-TW transition was found around $V_c$ [13], as shown in Fig. 2(g). Then the RTW moves faster ($|\theta| \gg 0$) with the increase of $V$. For a significantly higher $V$, the STMs (for $f < f_{TW}$ and $f > f_{TW}$) were indistinguishable and unmeasurable for $f_H$ because of our experimental limitations, i.e., the optical resolutions for the turbulent EC [Fig. 2(b)] and time-interval limitations for STMs.

There exist dislocations in the STMs; see the points guided by the broken-line arrows in Figs. 4 and 5. Sometimes, by increasing $V$, vortex-pair creation arises in the transient process, and then the wave number increases; the higher voltage appears to evoke the vortex-pair creation in earlier stages because of the perturbation due to the abrupt voltage change (Fig. 4), but its occurrence does not appear to exist at all times (Fig. 5). Such dislocations imply Benjamin-Feir instability [23,24], as is observed in binary-fluid Rayleigh-Bénard convections (RBCs) [25,26] and in rotating RBCs [27].

To elucidate the dependence of the TW on $V$, the Hopf frequency $f_H$ of the TW is given as a function of $V$ in Fig. 6. For $f < f_{TW} \approx 120$ Hz, $f_H$ monotonically increases from $f_H = 0$ (i.e., SW) with increasing $V$. For $f > f_{TW}$, it shows similar behavior but increases from finite values ($f_H \neq 0$, i.e., TW). According to this experimental result, $f_H$ can be roughly expressed as a simple function of $V$:

$$f_H = a[V - V_c(f_{TW})]^{\beta}, \quad V > V_c(f_{TW}) \quad \text{for TW}$$
$$f_H = 0, \quad V < V_c(f_{TW}) \quad \text{for SW}, \tag{1}$$

where $a \approx 0.6\,V^{-1}s^{-1}$, $\beta \approx 1$, and $V_c$ ($f_{TW} = 120$ Hz) $\approx 30$ V in this study. $f_H$ can be determined only by $V$ [$> V_c(f_{TW})$], being independent of $f$ ($> f_d \approx 50$ Hz in this study). This result should be compared to that of a 2DC

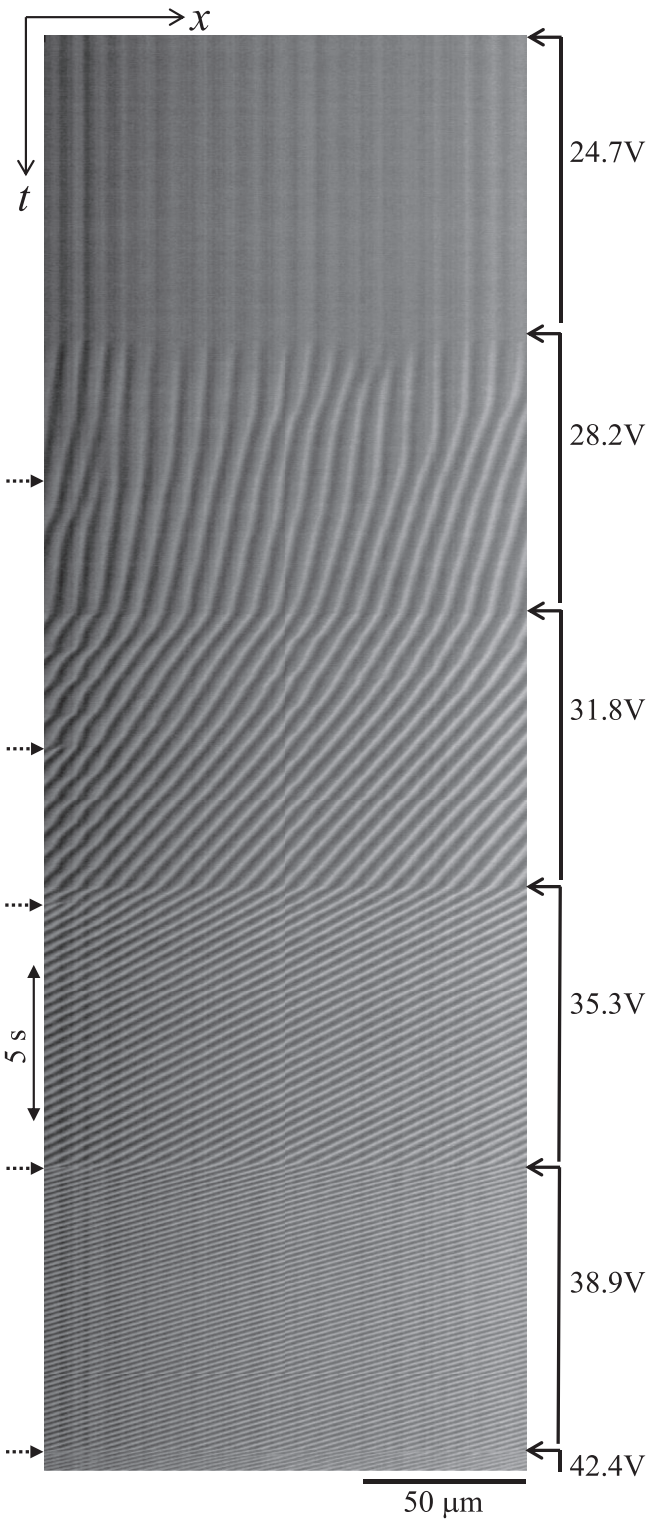


FIG. 4. STM with a steplike increase of the ac voltage $V$ (at a fixed frequency $f = 100$ Hz $< f_{TW} \approx 120$ Hz). An SW ($\theta = 0$) induced slightly above the EC threshold $V_c$ (= 24.1 V) evolves into a left-TW (LTW with $\theta > 0$) and becomes a more active TW with high $f_H$; for $f < f_{TW}$, TW arises as a secondary instability. See also Fig. 2(g). The broken-line arrow indicates the times of the appearance of dislocations resulting from EC vortex-pair creation (or annihilation).

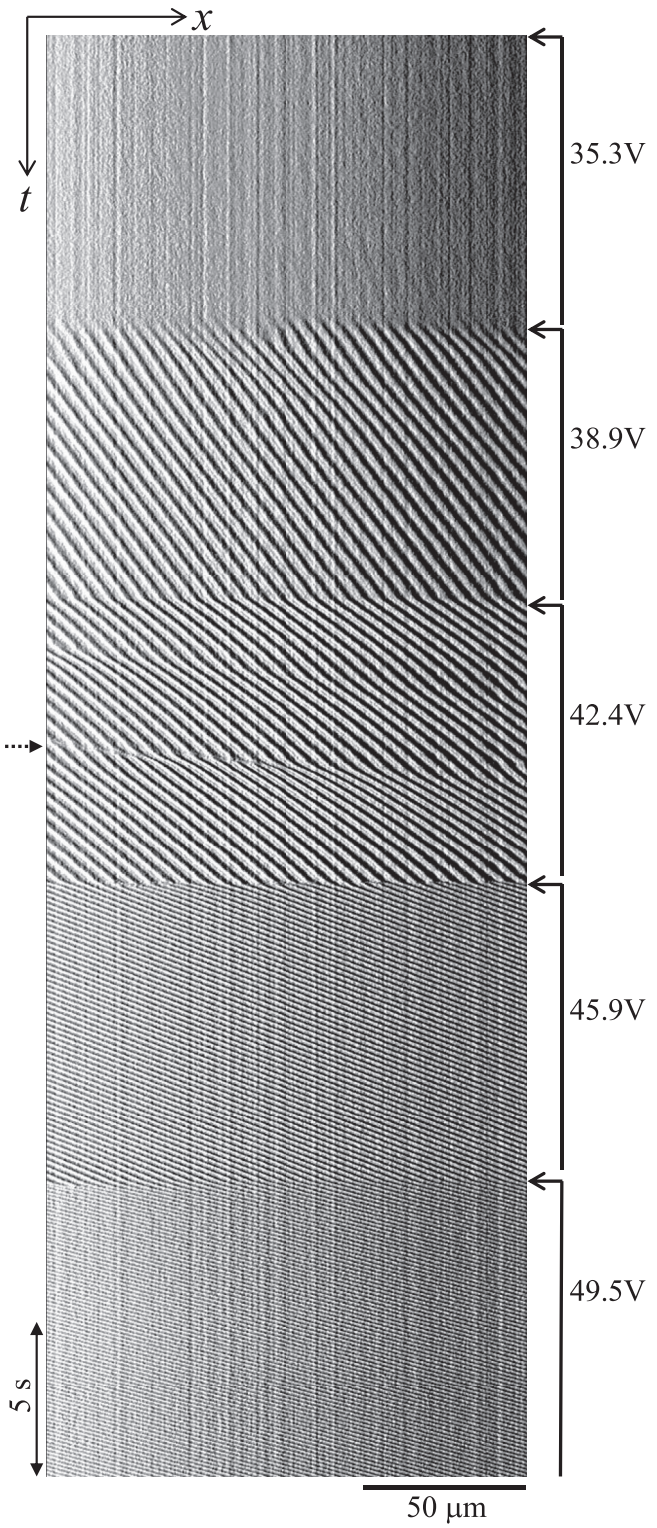


FIG. 5. STM with a steplike increase of the ac voltage $V$ (at a fixed frequency $f = 200\,\mathrm{Hz} > f_{\mathrm{TW}} \approx 120\,\mathrm{Hz}$). A TW (i.e., RTW) arises as a primary instability above the EC threshold $V_c$ (= 38.4 V) and develops into a more active TW with a high $f_{\mathrm{H}}$; no SW ($\theta = 0$) was observed below $V_c = 38.4\,\mathrm{V}$. See also Fig. 2(g). The broken-line arrow has the same meaning as those in Fig. 4.

showing a monotonous decrease with respect to $V$ [11]; the motion of the defects of EC rolls weakens the activeness of the TW in the 2DC, whereas such motion does not exist in the 1DC.

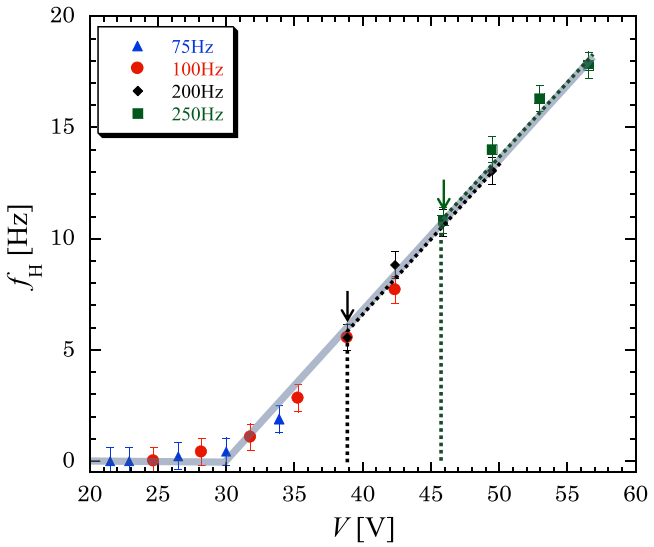


FIG. 6. Hopf frequency $f_{\mathrm{H}}$ of TW as a function of the ac voltage $V$. For $f = 75$ and 100 Hz ($< f_{\mathrm{TW}} \approx 120\,\mathrm{Hz}$), an SW ($f_{\mathrm{H}} = 0$) starts at $V_c$ and develops into a TW at $V_{\mathrm{TW}} \approx 30\,\mathrm{V}$, whereas a TW ($f_{\mathrm{H}} \neq 0$) suddenly starts at $V_c$ for $f = 200$ and 250 Hz ($> f_{\mathrm{TW}}$). See also Figs. 2(g), 4, and 5.

The transient dislocations in the 1DC differ from the incessant motion of defects in the 2DC. Furthermore, the TW ($f > f_{\mathrm{TW}}$) arises as a primary instability but the other ($f < f_{\mathrm{TW}}$) arises as a secondary instability; thus, the former can be explained by the WEM [10], whereas the latter lies outside of the WEM. As the WEM explains only a primary instability through a linear stability analysis [10], the SW-TW transition (for $f < f_{\mathrm{TW}}$) is a different problem.

### D. Noise-dependent TWs

To compare the aforementioned $V$-dependent TW with the $V_{\mathrm{N}}$-dependent TW, we measured $f_{\mathrm{H}}$ as a function of $V_{\mathrm{N}}$ using the same method. Figure 7 shows $f_{\mathrm{H}}(V_{\mathrm{N}})$ at a fixed reduced voltage $\varepsilon = (V^2 - V_c^2)/V_c^2 = 0.15$. $f_{\mathrm{H}}$ is almost independent of $V_{\mathrm{N}}$ for a low $V_{\mathrm{N}}$ ($<10\,\mathrm{V}$) but smoothly increases with the increase of $V_{\mathrm{N}}$ if $V_{\mathrm{N}}$ exceeds the characteristic intensity $V_{\mathrm{N}}^*$ (approximately 10 V). This result is very similar to that previously found in a 2DC; see Fig. 4 of Ref. [11]. That is, the TW can be reinforced only by the noise levels above an appropriate intensity ($V_{\mathrm{N}}^*$). In the case of a noise-dependent TW, the features of the TW are indistinguishable between a 1DC and a 2DC, as the defects are not dominant at a small $\varepsilon$ (= 0.01), even for a 2DC. Unlike these similar results for the 1DC and 2DC, the beating TW showing a modulation instability found in 2DCs (Fig. 6 in Ref. [11]) and in binary-fluid RBCs [28,29] was not observed in the present 1DC.

At a fixed large $V = 45.5\,\mathrm{V}$ (i.e., $\varepsilon = 0.35$ for $V_{\mathrm{N}} = 0$) and high $f = 200\,\mathrm{Hz}$ ($> f_{\mathrm{TW}}$), an STM was constructed with a steplike increase of $V_{\mathrm{N}}$. Figure 8 shows the result obtained between $V_{\mathrm{N}} = 21.5\,\mathrm{V}$ and 27.9 V. This STM indicates that by increasing $V_{\mathrm{N}}$, an active RTW ($\theta < 0$, $v > 0$) changes into an SW ($\theta = 0$, $v = 0$) around $V_{\mathrm{N}} = 24.7\,\mathrm{V}$ and then slowly evolves into an LTW ($\theta > 0$, $v < 0$) at $V_{\mathrm{N}} = 27.9\,\mathrm{V}$. Although the SW appears at some spaces, with the TW simultaneously

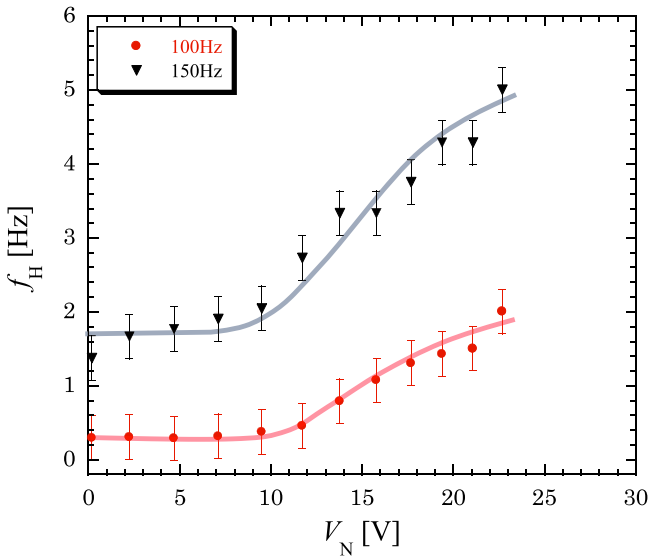


FIG. 7. Hopf frequency $f_H$ of a TW as a function of the noise intensity $V_N$ (at a fixed reduced voltage $\varepsilon = 0.15$) for $f = 100$ and 150 Hz. A TW with an almost constant low $f_H$ remains until a characteristic intensity of $V_N^* \approx 10$ V and then becomes faster with increasing $V_N$. The solid lines are for visual guidance.

arising at other spaces, its appearance requires it to change its traveling direction. To show SWs and TWs (i.e., RTW and LTW) in more detail, the light intensity $I(t,x_0)$ at a fixed $x_0$ is indicated in the right-hand side of the STM. Here one can differentiate SW* ($V_N = 26.3$ V) from SW ($V_N = 24.7$ V) by evaluating the $I(t,x_0)$ of both SWs; see Fig. 12 for details regarding SW and SW*. In the present study, such a change in the direction of the TW is uncontrollable but frequently occurs for a wide frequency range $f$ ($> f_d \approx 50$ Hz); such a phenomenon was also observed in a 2DC [11]. The reflection of the end wall may be a possible reason for the direction change of the TW, as observed in binary-fluid RBCs [28,29].

From the STM in Fig. 8, the $v$ and $f_H$ of the TW were measured as functions of the noise intensity $V_N$, as shown in Fig. 9. The $f_H(V_N)$ differs completely from that for the $V$ dependence (Fig. 6) and from that for the $V_N$ dependence under different $V$ conditions (Fig. 7). The velocity of the TW decreases with increasing $V_N$, and the Hopf frequency of the TW exhibits valley-shaped behavior against $V_N$. These results indicate that there exists an SW ($v = 0$, $f_H = 0$). Qualitatively, an almost $V_N$-independent TW (i.e., RTW) with a constant $v$ and $f_H$ maintains itself for a low $V_N$ ($< 20$ V), evolves into an SW around $V_N = 25$ V, and then reenters into a TW (i.e., LTW) with the opposite traveling direction. In addition, to differentiate the SW and SW* mentioned in Fig. 8, $v$ and $f_H$ are displayed for a fixed point $x_0$, where SW notably appears at an appropriate $V_N$, and for another point $x_1$ selected for SW*. In the case of $x_1$, no SW ($v = 0$, $f_H = 0$) appears to exist in the behavior of $f_H(V_N)$. This is because SW* occurs around $V_N = 25$ V, instead of SW. Owing to the small $|\theta|$ (or low $f_H < 2$ Hz) of SW*, one might be misled that SW* is still a TW. However, there exists a new factor inducing SW*, that is, an oscillation of EC vortices in contrast to the oscillation of EC rolls in the 2DC [11]; see Fig. 12(c) for details

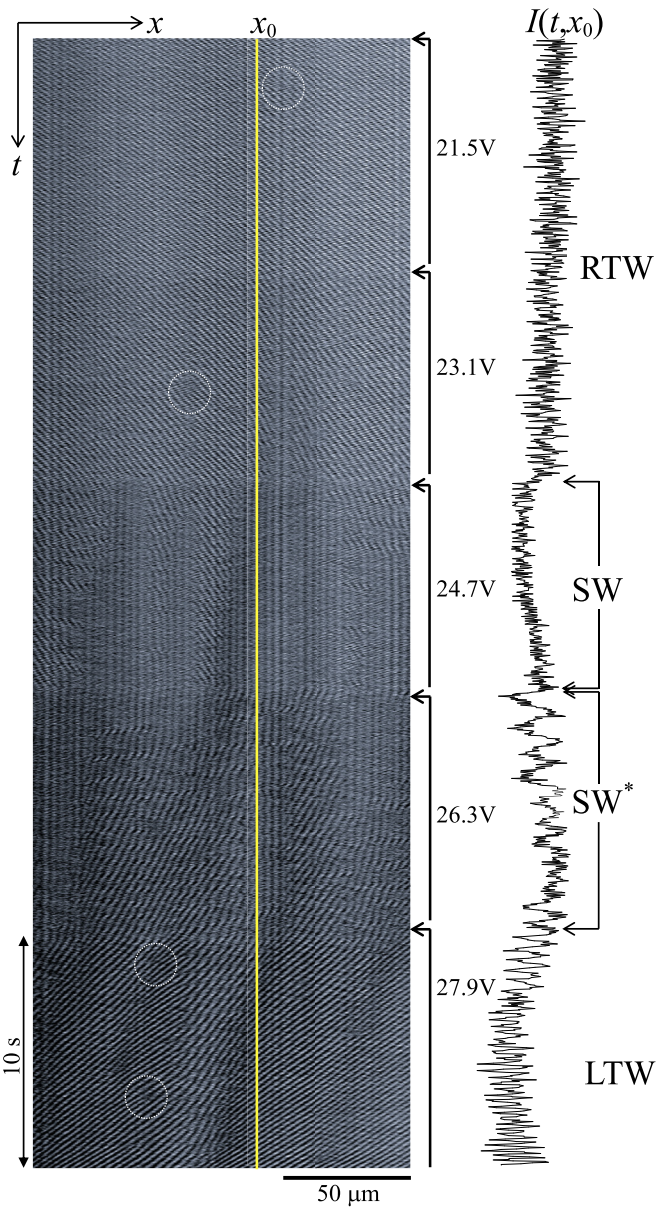


FIG. 8. STM with a steplike increase of the noise intensity $V_N$ (at fixed values of $V = 46.0$ V and $f = 200$ Hz). No noticeable variation of the STM was observed from $V_N = 0$ to 21.5 V; however, the STM shows a dramatic change of EC from $V_N = 23.1$ to 27.9 V. When $V_N$ is increased, the pattern evolution (RTW → SW → LTW) is observed; i.e., the traveling direction of TW is reversed after the appearance of an SW ($v = 0$). The transmitted light intensity $I(t)$ measured at a fixed point $x_0$ shows the evolution. See Fig. 12(c) for SW*.

regarding SW*. Within our experimental limits for measuring $v$ and $f_H$ ($V_N < 33$ V), $|v|$ and $f_H$ smoothly increase with $V_N$ ($>25$ V) after experiencing almost no variation and a smooth decrease to SW or SW* (for $V_N < 25$ V). For a significantly higher $V_N$ ($> 33$ V), the EC becomes turbulent, as shown in Fig. 2(b). Moreover, in the process of the perturbation from abrupt noise-intensity change, the dislocations are still found in Fig. 8, as revealed by the voltage change in Figs. 4 and 5. The creation and annihilation of vortex pairs are observed (e.g., inside the circles); thus, the wave number fluctuates.

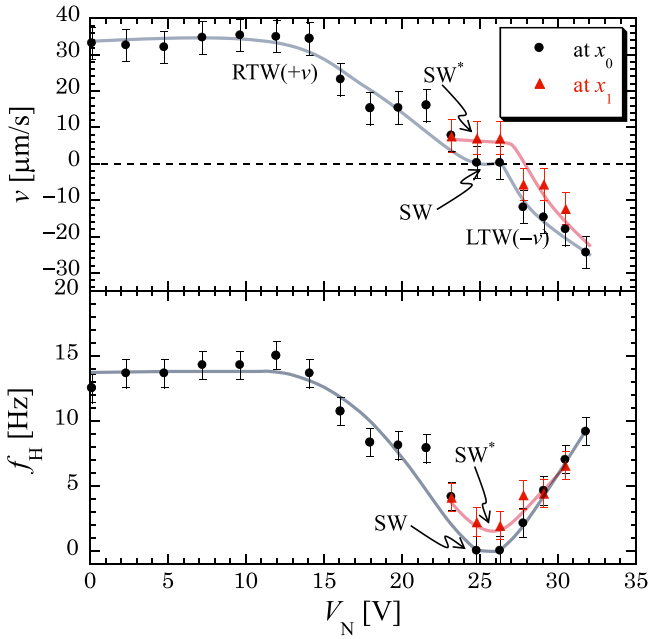


FIG. 9. Velocity $v$ and Hopf frequency $f_H$ of a TW with respect to the noise intensity $V_N$ (at fixed values of $V = 46.0\,\mathrm{V}$ and $f = 200\,\mathrm{Hz}$). At two fixed points ($x_0$,$x_1$), $v$ and $f_H$ were measured by increasing $V_N$. Around $V_N = 25\,\mathrm{V}$, a complicated EC (i.e., SW*) is observed with the typical SW ($v = 0$, $f_H = 0$); see also Figs. 8 and 12. SW and SW* are found at $x_0$ and $x_1$, respectively. The solid lines are for visual guidance.

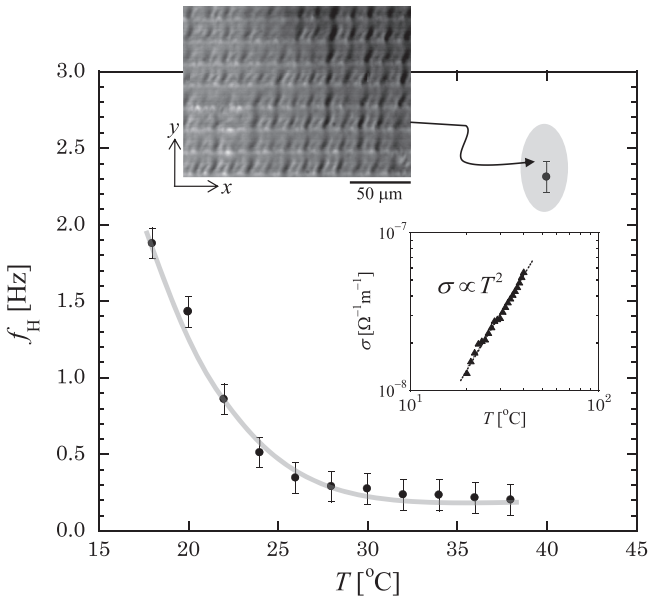


FIG. 10. Hopf frequency $f_H$ of a TW as a function of the temperature $T$ (at a fixed reduced voltage $\varepsilon = 0.15$ and $f = 100\,\mathrm{Hz}$). At $T = 40\,^\circ\mathrm{C}$ (near the nematic-isotropic point $T_{NI} \approx 43\,^\circ\mathrm{C}$), an unexpected $f_H$ was measured, which originated from the atypical TW displayed in the upper part. To validate the prediction of the WEM, the electrical conductivity $\sigma$ was measured as a function of $T$ using a 2DC containing the same NLC [11], as shown in the inset. See also Fig. 11. The solid lines are for visual guidance.

Additionally, it may be said that the Benjamin-Feir instability arises in the perturbation from abrupt noise-intensity change as well as from abrupt ac-voltage change [23–27].

### E. Temperature effects on TWs

In addition, we checked the TW in the 1DC by varying the temperature $T$ determining the electrical conductivity of the NLCs [4]. Figure 10 shows $f_H$ of TW as a function of $T$, which was measured at fixed values of $\varepsilon = 0.15$ and $f = 100\,\mathrm{Hz}$. The $f_H$ is qualitatively consistent with the prediction of the WEM ($f_H \propto \sigma^{-1/2} d^{-3}$) below $T = 40\,^\circ\mathrm{C}$ in consideration of $\sigma \propto T^2$, as shown in the inset of Fig. 10. However, the high temperature of $T = 40\,^\circ\mathrm{C}$ (near the nematic-isotopic transition temperature of $T_{NI} \approx 43\,^\circ\mathrm{C}$) violates the smooth monotonous behavior of $f_H$, as shown in Fig. 10. In this case, a different type of TW arises instead of the typical TW [Fig. 2(c)], exhibiting an abrupt increase of $f_H$ against the WEM; notice the new TW pattern in the upper part of Fig. 10. The separated EC along the $y$ axis resulting from the separated electrodes is synchronized in-phase and travels with an abnormally higher velocity and Hopf frequency than those measured at a typical reference temperature ($T = 25\,^\circ\mathrm{C}$). To illustrate this phenomenon, STMs for different temperatures are displayed in Fig. 11. For $T = 18\,^\circ\mathrm{C}$ (near the solid-nematic transition of temperature $T_{SN} \approx 17\,^\circ\mathrm{C}$), a typical TW shows a regular, typical STM [Fig. 11(a)]. When $T$ is increased, the TW develops into an SW-like wave ($v \approx 0$, $f_H \approx 0$) [Fig. 11(c)] and then evolves into the new TW mentioned above. A sign of the new TW is shown in Fig. 11(c), which is distinguishable from the typical SW [e.g., Fig. 4 for the present 1DC, or Fig. 2 of Ref. [11] for the previous 2DC]; notice the modulation of the $t$ axis. Other unknown properties of EC can probably generate such a new TW via reinforcing effects on the typical TW; whether this new TW relates to the mechanism of the WEM will be examined in the near future.

### F. Coexistence of TWs and SWs and soliton-like waves

In this section, we present some intriguing ECs, including SW and TW that are found in the 1DC only by employing the (comb-type) in-plane switching mode. Figure 12 shows coexistence of a TW and an SW in a single cell at fixed values of $V = 35.5\,\mathrm{V}$, $f = 100\,\mathrm{Hz}$, and $V_N = 29.5\,\mathrm{V}$; they always appear in alternate pattern shifts along the $y$ axis, as indicated in Fig. 12(a). For more detail, the corresponding STMs for the TW and SW are shown in Figs. 12(b) and 12(c), respectively. The TW exhibits the typical behavior with $v \approx 15\,\mu\mathrm{m/s}$ and $f_H \approx 4\,\mathrm{Hz}$. However, in the case of the SW, complicated behavior appears, similar to that of the SWs in Fig. 8. Normal SW segments appear in the STM; for example, there are several straight lines along the $t$ axis (i.e., $\theta = 0$) on the right-hand side of Fig. 12(c). The unique dynamics of the EC are also found in SW* formed between SW segments; see also SW* in Fig. 8. For SW*, the EC vortices appear to travel to the right-hand side in Fig. 12(c) as if they were a TW; however, they are completely different from the typical TW in Fig. 12(b). First, SW* is restricted to a narrow segment (approximately $10-50\,\mu\mathrm{m}$ in this study). Moreover, another periodicity is found for SW* along the $t$ axis; in fact, the EC vortices similar to the letter "I" (see Fig. 1) in the 1DC

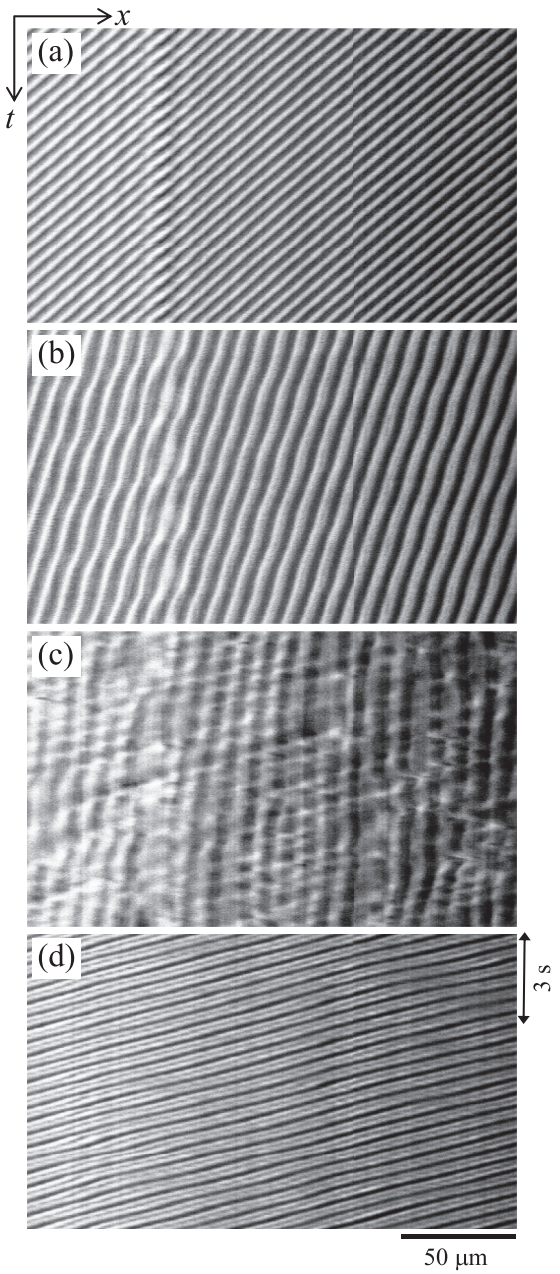


FIG. 11. STM at different temperatures $T$: (a) 18 °C, (b) 24 °C, (c) 38 °C, and (d) 40 °C. The STMs (a)–(c) show that the Hopf frequency of the TWs (i.e., LTW) decreased monotonically with increasing $T$ ($< 40$ °C); however, an unexpected TW (d) appears at $T = 40$ °C (near the nematic-isotropic transition temperature $T_{NI} \approx 43$ °C) after experiencing an SW-like wave (c) at $T = 38$ °C. See also Fig. 10.

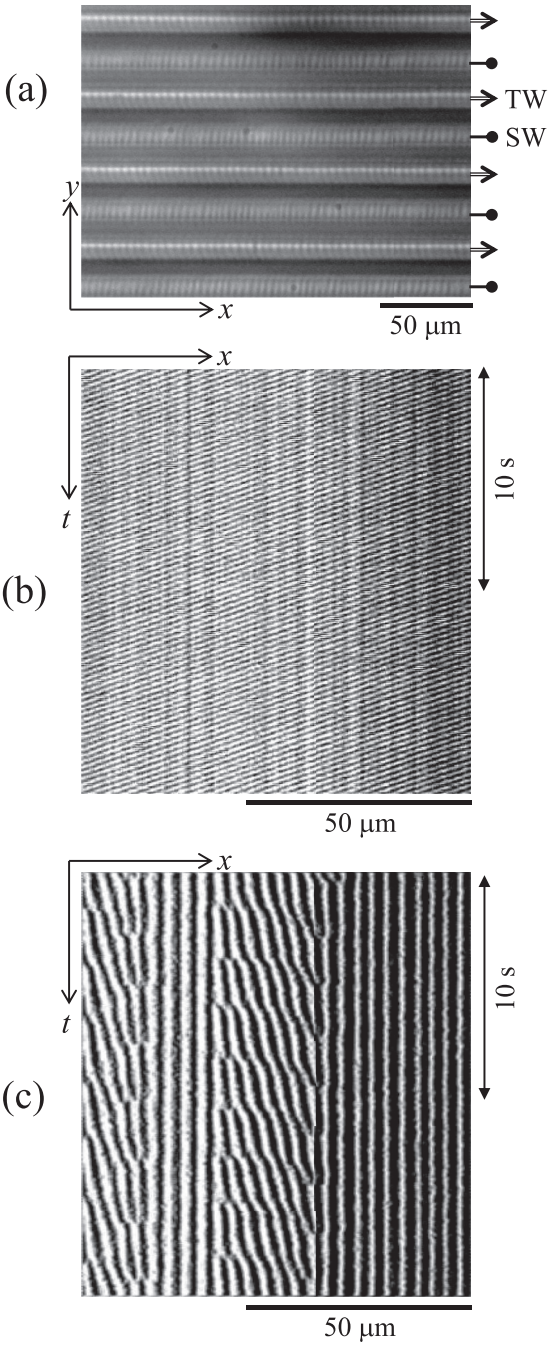


FIG. 12. Coexistence of a TW and an SW appearing in alternate pattern shifts along the $y$ direction at fixed values of $V = 35.5$ V, $f = 100$ Hz, and $V_N = 29.5$ V (a), as well as the STMs of the TW (b) and SW (c). The TW (i.e., LTW) is typical, whereas the SW is atypical; SW and SW* appear simultaneously in a single EC lane. Oscillating waves (i.e., SW*) are observed between typical SWs ($\theta = 0$, $f_H = 0$); e.g., see the SW* showing modulating EC in the middle of $X$. The two kinds of arrow symbols in (a) indicate TWs and SWs, respectively. See also Fig. 8 for SW*.

oscillate as an "X" with a period of $t_{osc}$ (approximately 1–2 s in this study), with the "I" alternately declining to the right- and left-hand sides. Such SW* accompanying such an oscillation was frequently observed for a relatively high $V$ and/or high $V_N$. Therefore, SW* should be distinguished from the normal SW found at a relatively low $V$ and/or low $V_N$ [see also Figs. 2(f) and 4], as well as from TWs.

Regarding SW*, note that the periodical motion of defects of EC rolls in the 2DC (Fig. 10 of Ref. [11]) plays a role in the variation of $f_H$ for the TW and can even cause a pattern change, such as a TW-SW transition [11]. In the present 1DC, the unaccountable oscillation of EC vortices may also play a similar role in the pattern formation and dynamics. Independent of the dimensions of the cells, another oscillation can arise and compete with the predominant oscillation phenomenon

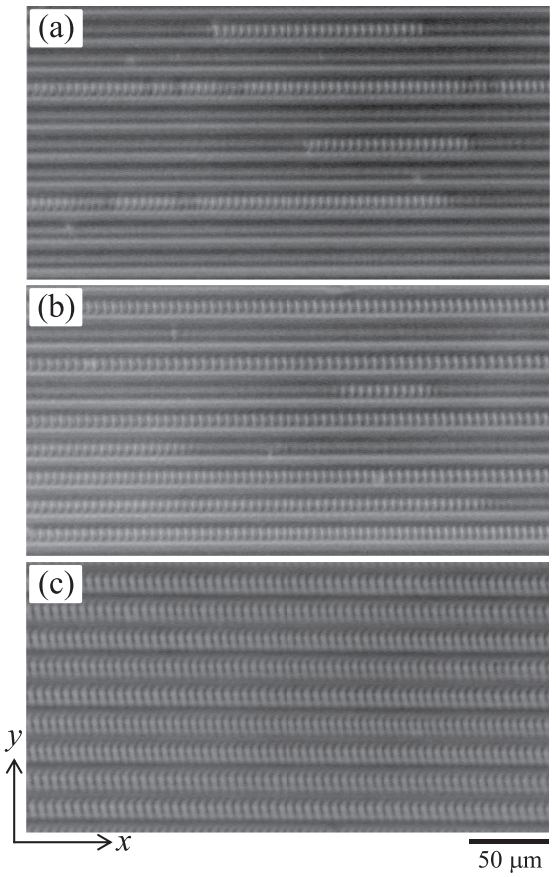


FIG. 13. Localized EC (i.e., SLWs) at $f = 250\,\mathrm{Hz}$ and $V = 56.8\,\mathrm{V}$ (a), 58.8 V (b), and 62.1 V (c). SLWs (a) with different lengths travel on the EC lanes; when $V$ is increased, they become a typical TW (c) by combining with each other (b). See also Fig. 14.

(i.e., TW explained by the WEM). The experimental results indicate that the new, secondary oscillation always weakens the primary one (i.e., TW), resulting in a slow TW and even an SW; however, the new SWs in the 1DC and 2DC developed in this way differ completely from the typical, normal SW found near the onset of EC.

In addition, one of the attractive EC patterns found in the 1DC is shown in Fig. 13. Localized EC, hereinafter called soliton-like waves (SLWs) showing traveling behavior, was frequently observed at high frequencies ($f > 2f_{\mathrm{TW}}$ in this study). When $V$ is increased, the SLWs [Fig. 13(a)] lengthen, combine with each other [Fig. 13(b)], and then develop into a typical TW [Fig. 13(c)]. A similar TW (referred to as "confined state") was observed in a binary-fluid RBC [29]. Furthermore, Fig. 14 shows an STM exhibiting the dynamics of the SLW displayed in Fig. 13(a). The dark regions indicate non-EC at the given time and space, whereas the gray ones show the dynamics of SLWs as localized TWs. The STM in Fig. 14 reads: an SLW appears at $t = 0$, and it travels to the right-hand side (with $v \approx 100\,\mu\mathrm{m/s}$ and $f_{\mathrm{H}} \approx 20\,\mathrm{Hz}$), and then the tail of the SLW appears at the left-hand side edge ($x = 0$) so that the non-EC maintains for a while; after few seconds ($< 3$ s, i.e., the width of the $t$ direction of black regions), the head of another SLW invades the non-EC space from $x = 0$; sometimes, the head of the SLW appears to be drawn at a certain non-EC space

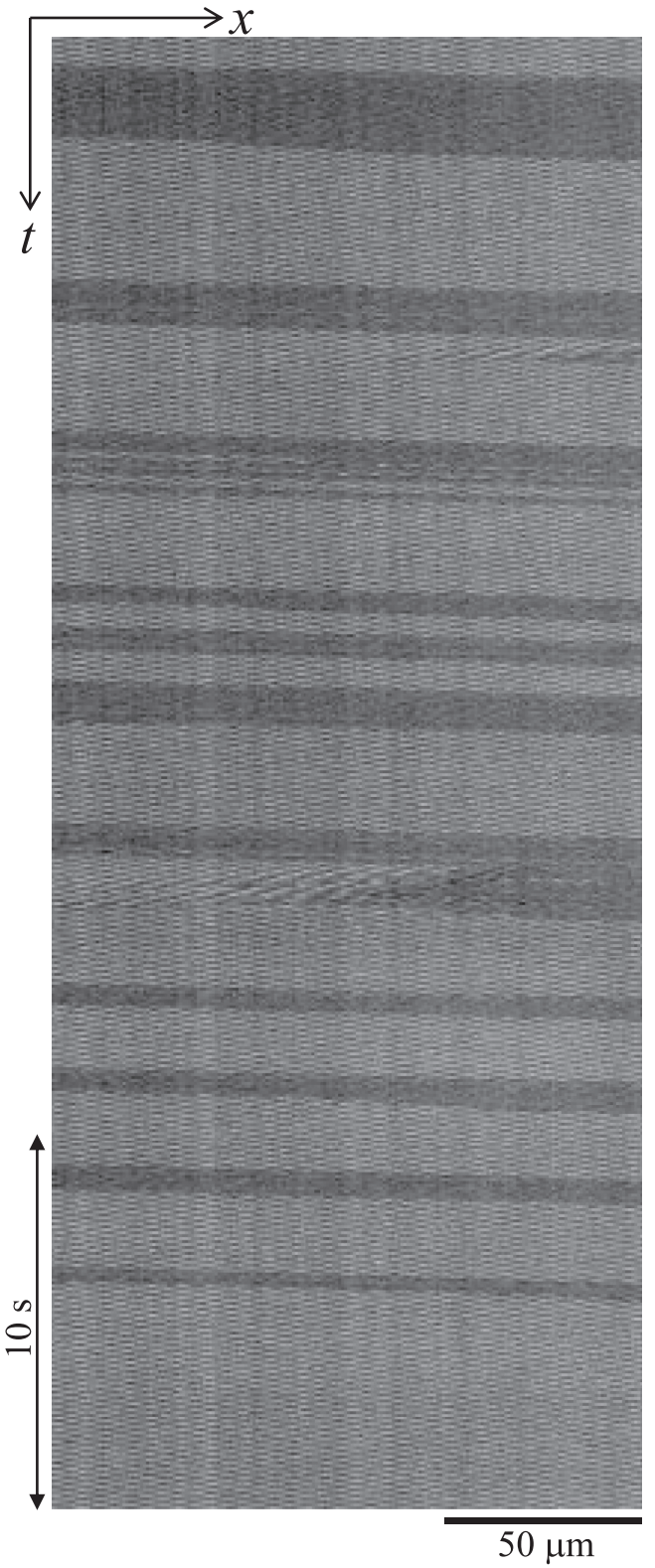


FIG. 14. STM for localized EC (i.e., SLW) at fixed values of $V = 56.8\,\mathrm{V}$ and $f = 250\,\mathrm{Hz}$, constructed using a single lane of Fig. 13(a). The dark regions indicate non-EC for time and space. Careful observation of these dynamics indicates that the SLWs travel towards the right-hand side with constant velocity. An SLW appears, travels (i.e., the gray region), and disappears, and then another appears at random time intervals (i.e., the width $\Delta t$ of the black region: $0.2\,\mathrm{s} < \Delta t < 3$ s in this study). See also Fig. 13.

that is not located at the right-hand side edge (e.g., see the dynamics around $t = 25$ s); such motion of the SLW appears to continue at random times. Such SLWs can be compared to the so-called "worms" frequently found in 2DCs [22,23]. A critical investigation of the SLWs is now in progress.

## IV. SUMMARY AND CONCLUSIONS

In 1DCs employing the in-plane switching mode, the EC was investigated in the presence and absence of external multiplicative noise. Regarding EC defects, the present 1DC should be differentiated from conventional 2DCs; this unconventional 1DC exhibiting "defect-free EC" is very useful for examining the fundamental features of EC because of its simplicity. In particular, this 1DC system can be used for the classical one-dimensional model dealing with convective instabilities; the EC in anisotropic fluids (i.e., NLCs) was first realized in a 1DC by employing the in-plane switching mode, while traditional Rayleigh-Bénard convections in isotropic fluids have abundantly been reported in 1DCs [25,26,28,29].

In this study, the characteristics of the TWs in 1DCs were investigated and compared with those found in 2DCs, where defects arise and act on the TWs. In particular, the Hopf frequency $f_H$ of the TWs was intensively examined at pure ac voltages $V$ and with a noise intensity of $V_N$ superposed on the ac field. The roles of these fields were clarified by comparing the results obtained for the 1DCs and 2DCs; the ac field linearly increases $f_H$, independent of the ac frequency $f$. The noise also increases it monotonically, but $f_H$ does not vary below a characteristic noise intensity $V_N^*$ (approximately 10 V in this study). The effect of the ac field on the TWs was elucidated in the 1DC, which may be misunderstood as a depressive effect on the TWs in the 2DC [13]. This is because the defects of EC in the 2DC cause disturbances that make it difficult to see the genuine effect of the ac field on TWs; however, the defect-free EC in the 1DC can clearly reveal this effect.

A variety of optical patterns in the 1DC were described in the frequency-voltage plane. By using STMs, the dynamics of the EC were examined; sometimes, a change of direction of the TW occurred with the appearance of an unexpected SW (i.e., SW$^*$) in the process of increasing the noise intensity $V_N$. SW$^*$ differs completely from a typical SW induced near the EC threshold. Unique EC vortices (oscillated in SW$^*$) and soliton-like waves were discovered in the 1DC; these can be compared to the oscillation of EC rolls and localized EC (referred to as "worms" in Refs. [14] and [30]) found in 2DCs, respectively. Moreover, several patterns and their dynamics observed in this study are very similar to those of binary fluid mixtures in 1DCs, such as rectangle cells [25,26,28,29,31] and annulus cells [31,32].

On the other hand, it has been found that the WEM suggested for Hopf bifurcation to a TW in the EC system [10] works in the present 1DC; the predicted Hopf frequency was validated in this experiment. However, the control of the TW directions, the secondary instability for the TWs beyond the EC threshold, the dependences of the Hopf frequency on the ac and noise fields, and the appearance of a new TW near a nematic-isotropic transition temperature ($T_{NI}$) remain as open problems.

Recently, the noise-induced dynamics in nonequilibrium systems have attracted considerable attention to exploiting the time-dependent nature and environment [33,34]. Beyond the physical system described in this study, noise-aided applications may be highly promising in various fields [12,35]. From this viewpoint, the noise-aided EC system gives us a hint for the practical applications via providing intriguing shifts of the dissipative patterns [13,36] and dynamics [11], as well as well-controlled shifts of the EC thresholds [13].

## ACKNOWLEDGMENT

This study was supported by JSPS KAKENHI (Grants No. 15K05215 and No. 18K03464).

[1] M. C. Cross and P. C. Hohenberg, Rev. Mod. Phys. **65**, 851 (1993).
[2] S. Kai, *Pattern Formation in Complex Dissipative Systems* (World Scientific, London, 1991).
[3] See reviews and references therein: e.g., T. John, J. Heuer, and R. Stannarius, Phys. Rev. E **71**, 056307 (2005); A. Buka, N. Eber, W. Pesch, and L. Kramer, Phys. Rep. **448**, 115 (2007).
[4] L. M. Blinov, *Electro-Optical and Magneto-Optical Properties of Liquid Crystals* (The Universities Press (Belfast), Belfast, 1983).
[5] E. F. Carr, Mol. Cryst. Liq. Cryst. **7**, 253 (1969).
[6] W. Helfrich, J. Chem. Phys. **51**, 4092 (1969).
[7] E. Bodenschatz, W. Zimmermann, and L. Kramer, J. Phys. (Paris) **49**, 1875 (1988); L. Kramer, E. Bodenschatz, W. Pesch, W. Thom, and W. Zimmermann, Liquid Cryst. **5**, 699 (1989).
[8] R. Williams, J. Chem. Phys. **39**, 384 (1963).
[9] See reviews and references therein: e.g., N. Eber, P. Salamon, and A. Buka, Liq. Cryst. Rev. **4**, 101 (2016).
[10] M. Treiber and L. Kramer, Mol. Cryst. Liq. Cryst. **261**, 311 (1995); M. Dennin, M. Treiber, L. Kramer, G. Ahlers, and D. S. Cannell, Phys. Rev. Lett. **76**, 319 (1996); M. Treiber and L. Kramer, Phys. Rev. E **58**, 1973 (1998).
[11] J.-H. Huh, Phys. Rev. E **95**, 042704 (2017).
[12] W. Horsthemke and R. Lefever, *Noise-Induced Transitions* (Springer-Verlag, Berlin, 1984); J. Garcia-Ojalvo and J. M. Sancho, *Noise in Spatially Extended Systems* (Springer-Verlag, New York, 1999).
[13] J.-H. Huh, Phys. Rev. E **84**, 025302(R) (2011); J. Phys. Soc. Jpn. **81**, 104602 (2012); J.-H. Huh and S. Kai, J. Phys. Soc. Jpn. Lett. **83**, 063601 (2014); J.-H. Huh, Phys. Rev. E **92**, 062504 (2015); J. Phys. Soc. Jpn. **85**, 024002 (2016).
[14] M. Dennin, G. Ahlers, and D. S. Cannell, Science **272**, 388 (1996); Phys. Rev. Lett. **77**, 2475 (1996); M. Dennin, D. S. Cannell, and G. Ahlers, Phys. Rev. E **57**, 638 (1998); N. Eber, P. Salamon, B. A. Fekete, R. Karapinar, A. Krekhov, and A. Buka, *ibid.* **93**, 042701 (2016).
[15] S. Kai, N. Chizumi, and M. Kohno, J. Phys. Soc. Jpn. **58**, 3541 (1989).
[16] P. Toth, N. Eber, T. M. Bock, A. Buka, and L. Kramer, Europhys. Lett. **57**, 824 (2002).

[17] M. Oh-e and K. Kondo, Appl. Phys. Lett. **67**, 3895 (1995).
[18] A. K. Bbowmik, Z. Li, and P. J. Bos, *Mobile Displays* (Wiley, New York, 2008).
[19] J.-H. Huh, in *Proceedings of 2017 International Conference on Noise and Fluctuations* (ICNF 2017, Vilnius, Lithuania) (2017).
[20] J.-H. Huh and S. Kai, Phys. Rev. E **68**, 042702 (2003).
[21] J.-H. Huh, J. Phys. Soc. Jpn. **78**, 043601 (2009).
[22] S. Kai and W. Zimmermann, Prog. Theor. Phys. Suppl. **99**, 458 (1989).
[23] T. B. Benjamin and J. E. Feir, J. Fluid Mech. **27**, 417 (1967).
[24] J. T. Stuart and R. C. Diprima, Proc. R. Soc. Lond A **362**, 27 (1978).
[25] P. Kolodner, Phys. Rev. A **46**, R1739(R) (1992).
[26] P. Kolodner, Phys. Rev. A **46**, 6431 (1992).
[27] Y. Liu and R. E. Ecke, Phys. Rev. Lett. **78**, 4391 (1997).
[28] C. M. Surko and P. Kolodner, Phys. Rev. Lett. **58**, 2055 (1987); P. Kolodner, C. M. Surko, and H. Williams, Physica D **37**, 319 (1989).
[29] V. Steinberg, J. Fineberg, E. Moses, and I. Rehberg, Physica D **37**, 359 (1989).
[30] Y. Tu, Phys. Rev. E **56**, R3765 (1997); H. Riecke and G. D. Granzow, Phys. Rev. Lett. **81**, 333 (1998).
[31] J. J. Niemela, G. Ahlers, and D. S. Cannell, Phys. Rev. Lett. **64**, 1365 (1990).
[32] P. Kolodner, Phys. Rev. A **44**, 6448 (1991).
[33] L. Ridolfi, P. D'Odorico, and F. Laio, *Noise-Induced Phenomena in the Environmental Sciences* (Cambridge University Press, Cambridge, 2011).
[34] D. S. A. Simakov and J. Pérez-Mercader, Sci. Rep. **3**, 2404 (2013).
[35] F. Sagués, J. M. Sancho, and J. García-Ojalvo, Rev. Mod. Phys. **79**, 829 (2007).
[36] J.-H. Huh, Phys. Rev. E **94**, 052702 (2016).